THE PADME EXPERIMENT

P. Albicocco (AdR), F. Bossi, B. Buonomo, E. Capitolo (Tec.), C. Capoccia (Tec.),
S. Ceravolo (Tec.), G. Corradi (Tec.), R. De Sangro, D. Domenici, G. Finocchiaro,
L.G. Foggetta, G.S. Georgiev (Ass.), A. Ghigo, F. Giacchino (AdR), P. Gianotti (Resp.),
V. Kozhuharov (Ass.), B. Liberti, M. Martini (Ass.), A. Saputi (Tec.), I. Sarra (Ass.), B. Sciascia,
T. Spadaro, E. Spiriti, C. Taruggi (Dott.), E. Vilucchi

1 Introduction

One of the most intriguing mysteries in physics today, is that the matter seen in the universe accounts only for about 5% of the observed gravity. This has triggered the idea that enormous amounts of invisible dark matter should be present.

Among the different theoretical models that try to define what dark matter could be, there are those that postulate the existence of a “Hidden Sector” populated by new particles that do not couple with those of the Standard Model (SM). The only connection within these 2 worlds could be realized by a low-mass spin-1 particle, indicated with the symbol A', that would possess a gauge coupling of electroweak strength to dark matter, and a much smaller coupling to the SM hypercharge [1]. This Dark Photon (DP) could be the portal connecting ordinary and dark world.

The PADME experiment aims to search for signals of such a DP studying the reaction:

$$e^+e^- \to \gamma A'$$

using the positron beam of the LNF LINAC and identifying the A' as a missing mass signal.

PADME (Positron Annihilation into Dark Matter Experiment) is an international collaboration of about 50 people that involves, in addition to LNF researchers, scientists from the INFN sections of Roma1, Roma2 and Lecce, the Sapienza and Tor Vergata Universities of Rome (IT), the Salento University (IT), the Sofia University (BG), the Cornell University (USA), and the Atomki Institute of Debrecem (H).

The apparatus, built and installed in 2018, had a commissioning data taking from October 2018 to February 2019.

2 The PADME experiment

The goal of the PADME experiment is to search for DPs produced in the annihilation process of the positron beam of the LNF LINAC with a thin diamond target and then identified using a missing mass technique [2].

Figure 1 shows a scheme of the apparatus whose basic elements are:

- a high intensity and low divergence positron beam, impinging on a thin, active target, capable of monitoring the beam size and intensity;
- a vacuum chamber to avoid spurious particle interactions;
- a magnet to deflect the beam of positrons emerging from the target, with the additional task of allowing the measurement of the momentum of the interacting positrons, thus improving the rejection of the Bremsstrahlung background;

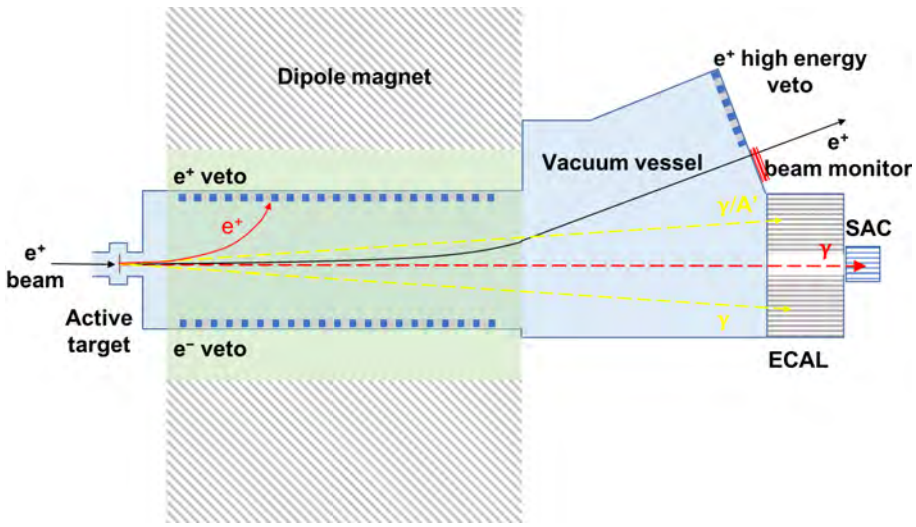

Figure 1: *The PADME experiment layout. From left to right: the active target, the positron/electron vetoes inside the magnetic field, the high energy* e$^+$ *veto near the non-interacting beam exit, the e.m. calorimeters (ECal, SAC), the solid state beam monitor detector.*

- a finely-segmented, high-resolution e.m. calorimeter, to measure the momentum of the single SM photons (ECal).

Since the processes that mainly take place in the beam-target interaction are Bremsstrahlung and $e^+e^- \to \gamma\gamma(\gamma)$, to cut out these background events, two extra components are crucial:

- a fast Small Angle Calorimeter (SAC), placed behind the central hole of the primary one. This is used to detect and veto backgrounds photons (mainly from Bremsstrahlung);

- three stations of plastic scintillator slabs, located inside the vacuum chamber, two within the dipole magnet gap (Pveto and Eveto), and the third one on the beam exit (HEPveto), to veto charged particles produced in the interaction.

To have a more accurate monitoring of the beam, in the target region are installed two planes of silicon pixel detectors placed up and down stream the active diamond target. Each plane consists of two MIMOSA 28 Ultimate chips, developed for the upgrade of the STAR vertex detector [3]. These devices integrate a Monolithic Active Pixel Sensor (MAPS) with a fast binary readout. Each sensor consists of a matrix of 928×960 pixels of 20.7 μm side with a thickness of 50 μm. For the STAR experiment the chips, that dissipate 150 mW/cm^2, operate in air without cooling. For PADME, the detector has been placed in vacuum and a modified PCB has been developed by the LNF electronic service to provide cooling. In the following sections more details on the detector characterization are given.

The MIMOSA detector cannot stay on the beam line during the data taking, therefore an extra monitoring device is placed out of the vacuum on the positron beam exit trajectory. This is an array (6×2) of Timepix3 chips [4] able to record either the time-of-arrival (ToA) and the energy of the incident particles providing excellent energy and time resolutions. A single silicon chip is designed in 130 nm CMOS technology and contains 256×256 pixels (55×55 μm^2). This detector has been build ad installed at LNF by the ADVACAM company [5].

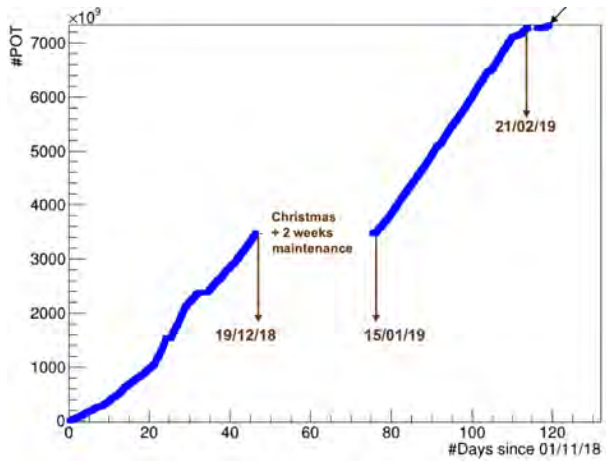

Figure 2: *Data collected by PADME during the commissioning data taking.*

The physics potential of the PADME experiment extends beyond DP search. The built detector is also sensitive to any new light particle, including scalars and pseudo-scalars, that are produced in the positron-on-target interaction. An estimate of the physics potential of PADME to search for axion like particles as well as other exotic states is ongoing. In addition, it will be possible to perform measurements of the differential cross sections for Bremsstrahlung emission for positrons in the $O(100$ MeV$)$ energy range and to address the multi-photon annihilation cross sections.

3 Activity of the PADME LNF group

The starting of 2019 saw the PADME collaboration involved in the commissioning data taking of the experiment that took place from October 2018 to February 2019. The main goal of this data collection was to define the best beam conditions and to calibrate the detector components

The PADME experiment uses the positron beam coming from the LNF LINAC. The beam line is the former BTF line 1, that since October 2018 is exclusively dedicated to the experiment. Positrons can be accelerated up to 550 MeV after being generated in the LINAC on a W-Re converter of 2 X_0 (Positron converter) located after the first electron accelerating sections (primary positron beam) or can be produced by a primary electron beam of 750 MeV hitting a Cu converter of selectable X_0 (1.7, 2, or 2.3) (BTF target) located before a 1 m thick concrete wall that separate the LINAC from the BTF experimental hall (secondary positron beam). An energy selection system, and some collimators on the BTF transfer-line, define momentum, spot size, and intensity. Figure 3 shows the details of the PADME beam line.

The majority of the data collected during this first run were acquired with the positrons produced at BTF target and only few days, at the end of February 2019, were instead collected with the primary positron beam.

The analysis of the data showed that the level of background induced by the beam in the PADME setup was extremely high, above all for the data-set collected with the secondary beam (see fig. 4). Therefore, it was foreseen an other technical run of four weeks for July 2019, to study the best beam setup before starting the real data taking in Autumn. Due to problems at the air conditioning system of BTF hall and to the breaking of a Be-window that separated the accelerator vacuum from that of the experiment, the program was canceled and the PADME data taking has been postponed to 2020.

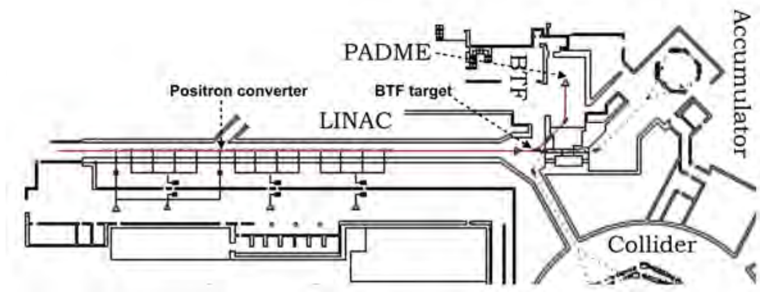

Figure 3: *Layout of the PADME beam line.*

4 Detector calibration

The data set collected in the commissioning run has been intensively analyzed in order to calibrate detector responses and to start extracting first physics results.

The active diamond target was performing very well. Figure 5 shows the beam profiles (x,y) measurements. Only one of the 16 strips on the x side is not giving signal, but its information can be reconstructed interpolating the signals of the adjacent ones.

PADME target can also provide particle-beam multiplicity, by measuring the deposited charge. Figure 6a shows the results of the target calibration performed using as a reference the signal of a Lead-Glass fully containing Cherenkov detector. The response linearity was constantly monitored during the data taking. Figure 6b reports the result of two measurements performed in different days showing optimum detector stability.

The three stations of the charged particles veto, due to the high density of positrons in the beam bunch ($\sim$ 20k in 200 ns), experienced high rates. Figure 7 shows a typical signal of several of the Pveto sticks. More than one particle can hit the same channel and therefore multi-hit reconstruction algorithms have been developed to properly distinguish them. The hit position gives a rough estimate (2%) of the particle momentum and performing a time correlation between Pveto and SAC energy deposit, it is possible to select Bremsstrahlung events. Figure 7b shows this correlation plot. The picture has been obtained subtracting the background measured in a dedicated run with the target off beam.

In order to monitor constantly the response of ECal, a cosmic ray trigger has been implemented. Two scintillator slabs ($50\times10\times3$ cm^3) were installed above and below the calorimeter. The signals of both ends of the scintillators are combined to define the trigger signal corresponding to cosmic rays. Figure8 shows a cosmic ray track in ECal, the calorimeter response to m.i.p. and the efficiency of each unit. Only 4 calorimeter crystals, out of 616, were not working (white spots in the figure) and will be fixed before the data taking. To evaluate the efficiency of the crystals, triplets of superimposed units were considered. With this method the peripheral crystals and those surrounding the central hole cannot be monitored. Cosmic-ray triggers were interleaved with physical events during the whole data taking.

To determine the calorimeter energy resolution, a special data taking was performed with the target off beam and firing a single-positron directly on ECal. Figure 9 shows the reconstructed energy spectrum with superimposed a Gaussian fit. Since the beam multiplicity was not rigorously one a second peak, corresponding to two positrons hitting the calorimeter, is present on the right side of the main spectrum. The measured energy resolution (2.7 %) is better than what was measured in test beams with detector prototypes.

Figure 10 shows the preliminary results of the analysis of $e^+e^- \rightarrow \gamma\gamma$ events. The red histogram is the sum of the energies of the two photons in the final state and shows a peak at the

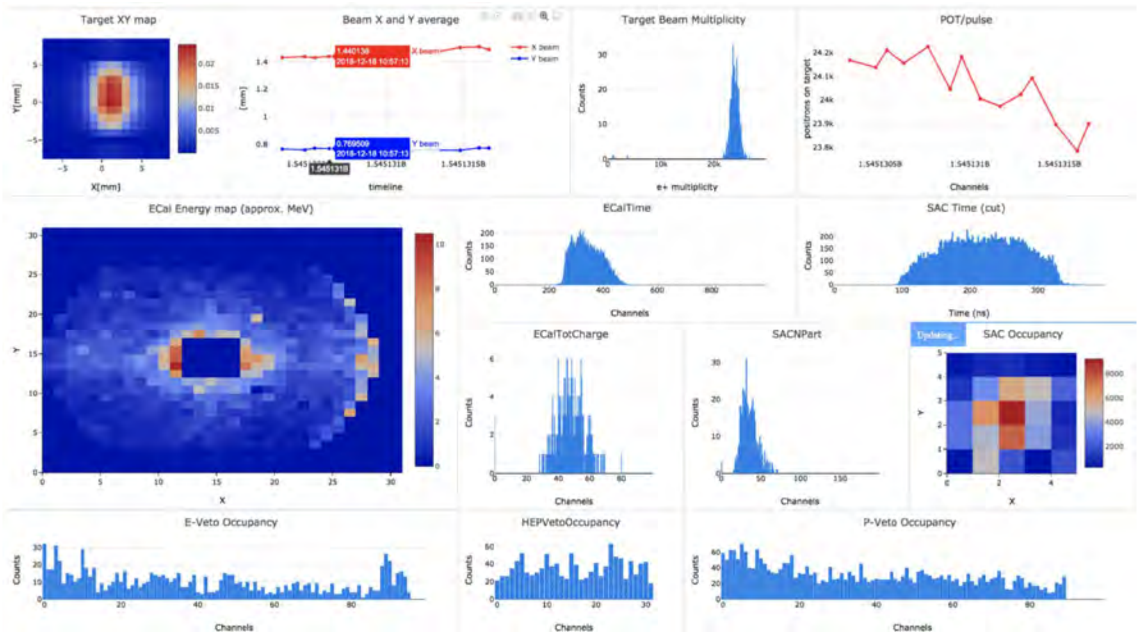

Figure 4: *Screenshot of the PADME online monitor. All main information from each detector is available in a single web page to control running conditions. High levels of backgrounds are visible in ECal, above all around the central hole.*

beam energy. The blue one corresponds to a data taking with target off beam and can be used to evaluate the level of background.

Concerning computer resources, the PADME experiment consolidated its activity on the Tier-2 farm available at LNF. Raw, MC and reconstructed data are collected in the storage system while MC running, reprocessing and analysis jobs can use the Tier2 cluster, with pledged resources of about 1.1 PB of storage tape, about 300 TB of storage disk and 6.7 HS06 of computing power.

5 Beam induced background

The collection of the first PADME data-set showed an unexpected source of beam-induced background leading to a large deposition of energy in ECal. This background is higher when the experiment ran with the secondary beam, but even with the primary one it is not negligible. Therefore, additional MC studies were performed in order to understand the origin of this extra deposit and to find out a way to eliminate it. A detailed MC of all the components of the beam line was implemented in order to reproduce the data and to understand which changes had to be introduced. Figure 11 shows the layout of the simulated setup. In the picture are indicated the different points where the beam spot can be checked (Flag #).

From this analysis two main sources of background were identified: the Beryllium window that separated the accelerator vacuum from the detector vacuum, and the magnet that steers the beam from the injection point into the PADME target (red dipole in fig. 11). The forthcoming PADME data taking will see a completely new beam-line. The Be window will be removed and to separate the two different vacuum regions it will be used a thinner Mylar window placed more upstream.

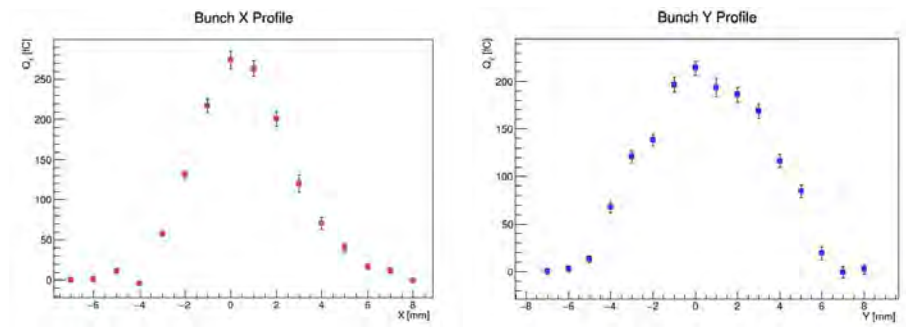

(a) (b)

Figure 5: *Beam bunch profiles: a) x coordinate b) y coordinate. Only strip n. 4 on the x side is not giving signal.*

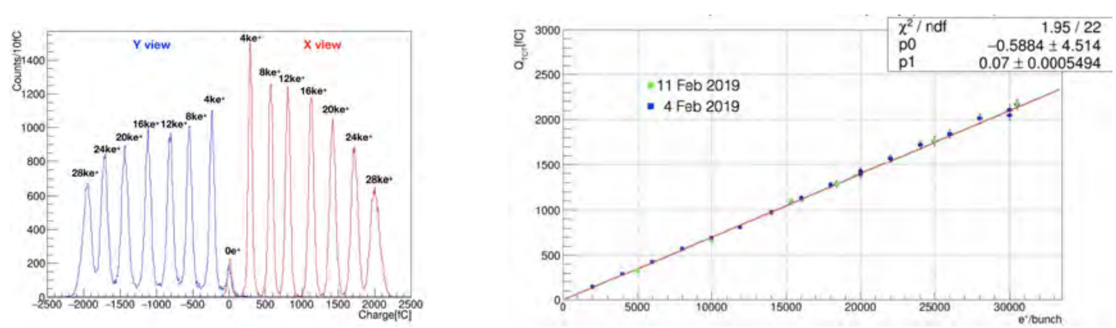

(a) (b)

Figure 6: *a) Total collected charge on x and y target sides for different bunch multiplicities. b) Charge multiplicity correlation. Data points of different colours refer to measurements performed in different days.*

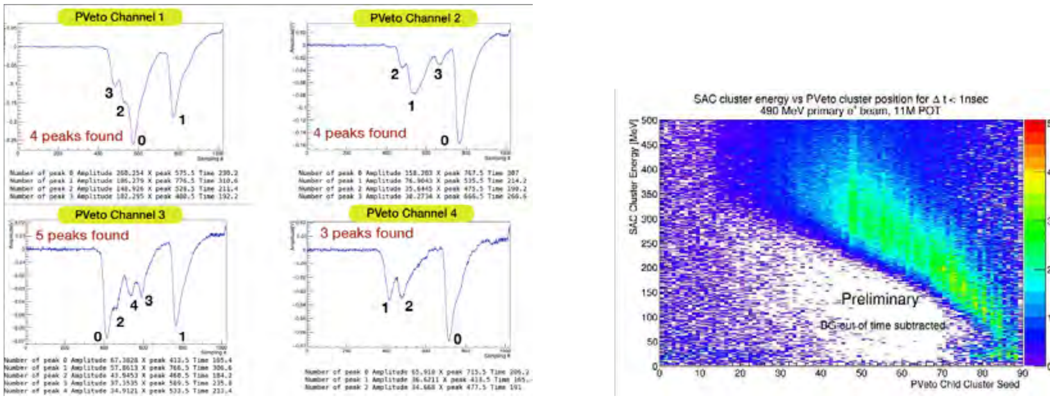

(a) (b)

Figure 7: *a) Waveforms of different slabs of the Pveto showing the presence of more than one particle. Multi-hit algorithms have been implemented in the data analysis. b) Correlation between Pveto hit slab and SAC measured energy. Background, evaluated in a dedicated run with target off beam, has been subtracted. Bremsstrahlung signals are clearly visible. Beam characteristics and correlation time are indicated on top of the picture.*

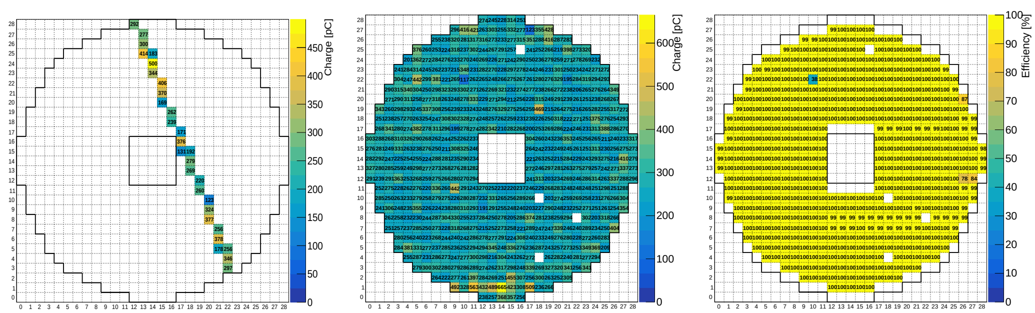

(a) (b) (c)

Figure 8: *a) Track of a cosmic ray crossing the calorimeter. The numbers indicate the charge measured by each unit in pC. b) Calorimeter layout showing for each unit the Most Probable Value (MPV) of the charge released by cosmic rays. The average value 266±1.4 pC corresponds to an energy release of abount 18 MeV. c) Efficiency plot of the calorimeter units. The average value exceeded 99.8 %. The method adopted does not allow to determine the efficiency of peripheral crystals (see text for more details).*

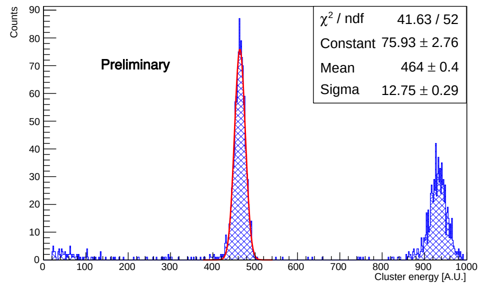

Figure 9: *Energy resolution of ECal measured in a dedicated run with single positrons firing in the calorimeter. The beam multiplicity is not rigorously one, then a second peak, corresponding to two positrons, is present on the right.*

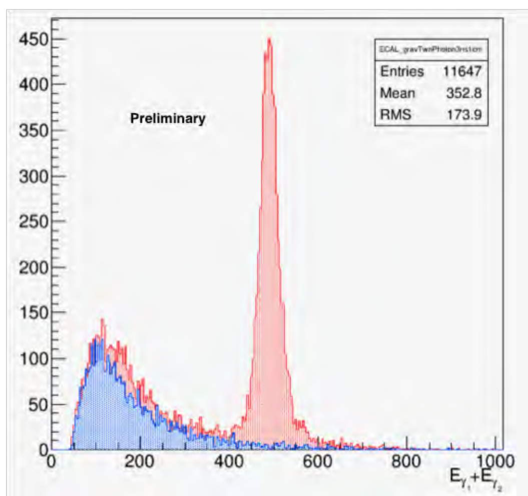

Figure 10: *Total energy measured in ECal for events with two photons in the final state (red). Blue histograms corresponds to background (see text for more detail).*

6 List of Conference Talks by LNF Authors in Year 2019

Here below, it is the list of conference presentations given by LNF PADME members:

1. V. Kozhuharov, "Searching for dark sector with missing mass technique in fixed target", International Workshop e^+e^- Collisions From Phi to Psi 2019, Novosibirsk, 25 Feb. - 1 Mar. 2019.

2. C. Taruggi, "The PADME experiment at LNF", International Conference on the Structure and Interactions of the Photon (PHOTON19), Frascati, 3 - 7 Jun. 2019.

3. F. Giacchino, "A Light Dark Matter Portal: the axion-like particle", International Conference on the Structure and Interactions of the Photon (PHOTON19), Frascati, 3 - 7 Jun. 2019

4. P. Gianotti, "Search of a low energy Dark Photon: The PADME experiment", 19^{th} Lomonosov Conference on Elementary Particle Physics, Moscow, 21 - 28 Aug. 2019.

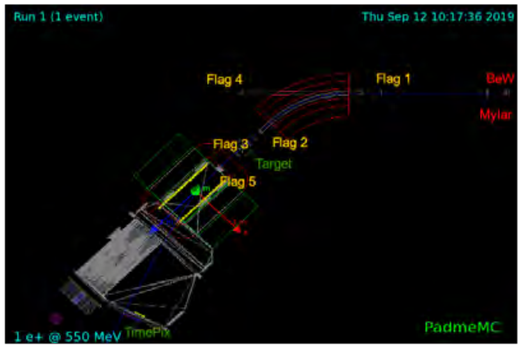

Figure 11: *Layout of the PADME setup and of the beam-line used to perform MC simulations devoted to beam induced background study. The labels Flag # indicated the points where beam spot can be checked.*

5. V. Kozhuharov, "Searching for new light particles with positrons on target", Light Dark Matter Accelerators, Venezia, 20 - 22 Nov. 2019.

For the complete list of presentations to conferences given by the PADME collaborators, refer to `http://padme.lnf.infn.it/list-of-papers/`.

7 List of Publications by LNF Authors in Year 2019

Here below, it is the list of papers published by PADME LNF members in 2019:

1. A. Frankenthal *et al.*, "Characterization and performance of PADME's Cherenkov-based small-angle calorimeter", Nucl. Instrum. Meth. **A919** (2019) 89-97.
2. S. Ivanov, V. Kozhuharov, "The charged particle veto system of the PADME experiment", AIP Conf. Proc. 2075 (2019) no.1, 080005.
3. V. Kozhuharov, "The PADME experiment at LNF-INFN", AIP Conf.Proc. 2075 (2019) no.1, 080008.
4. P. Gianotti, "The calorimeters of the PADME experiment", Nucl. Instrum. Meth. **A936** (2019) 150-151.
5. P. Gianotti,"The investigation on the dark sector at the PADME experiment", Nucl. Instrum. Meth. **A936** (2019) 266-267.
6. C. Taruggi, "The PADME experiment at INFN LNF", Frascati Physics Series **69** (2019) 188.
7. F. Giacchino, "A Light Dark Matter portal: the Axion-like Particle", Frascati Physics Series **69** (2019) 205.

The complete list of papers published by the PADME collaboration in 2019 can be find here `http://padme.lnf.infn.it/papers/`.

References

1. B. Holdom, Phys. Lett. B 166, 196 (1986).
   M. Pospelov, Phys. Rev. D 80, 095002 (2009).

2. M. Raggi and V. Kozhuharov, Rivista del Nuovo Cimento 38 no. 10, (2015).
   DOI 10.1393/ncr/i2015-10117-9

3. I. Valin *et al.*, JINST 7, C01102 (2012).

4. T. Poikela *et al.*, JINST 9, C05013 (2014).

5. ADVACAM s.r.o., U Pergamenky 12, 17000 Praha 7, Czech Republic, (`https://advacam.com`).